Defects and hyperfine interactions in Ni–Y intermetallics (Y = Al, Ga, In, Ti) via ^{27}Al, ^{47}Ti, ^{61}Ni, ^{69,71}Ga and ^{115}In nuclear resonance

2003 J. Phys.: Condens. Matter 15 8389

(http://iopscience.iop.org/0953-8984/15/49/016)

INSTITUTE OF PHYSICS PUBLISHING JOURNAL OF PHYSICS: CONDENSED MATTER

J. Phys.: Condens. Matter **15** (2003) 8389–8406 PII: S0953-8984(03)67995-6

Defects and hyperfine interactions in Ni–Y intermetallics (Y = Al, Ga, In, Ti) via ^{27}Al, ^{47}Ti, ^{61}Ni, ^{69,71}Ga and ^{115}In nuclear resonance

T J Bastow and G W West

CSIRO Manufacturing and Infrastructure Technology, Private Bag 33, S Clayton MDC, Clayton, Victoria 3169, Australia

Received 26 August 2003
Published 25 November 2003
Online at stacks.iop.org/JPhysCM/15/8389

Abstract

Defect structures and nuclear electric hyperfine interactions have been investigated in a series of binary Ni–Al, Ni–Ga, Ni–In intermetallic compounds, and the shape memory compound NiTi using ^{27}Al, ^{47,49}Ti, ^{61}Ni, ^{71}Ga and ^{115}In nuclear resonance. Components of the ^{61}Ni NMR spectrum for a series of cubic $Ni_{1-x}Al_x$ and $Ni_{1-x}Ga_x$ specimens on either side of $x = 0.5$ have been identified as due to Ni substitutions and Al (or Ga) vacancies. For stoichiometric NiAl, Ni_2Al_3 and $NiAl_3$ the ^{61}Ni lines are narrow and distinguished by well-separated Knight shifts, although the ^{61}Ni lineshape for the ordered vacancy compound Ni_3Al_4 indicates a substantial nuclear quadrupole interaction at the Ni site.

The substitution for Al of the group III elements Ga and In, which have isoelectronic outer shells, acts to increase the ^{61}Ni Knight shift such that $^{61}K(Al) < {}^{61}K(Ga) < {}^{61}K(In)$. This trend is observed not only for cubic NiAl and NiGa, but also for trigonal Ni_2Al_3, Ni_2Ga_3 and Ni_2In_3.

In NiTi the sharp first-order transition between the (high-temperature) cubic phase and the (low-temperature) monoclinic phase has been observed while monitoring the ^{61}Ni and ^{49,47}Ti NMR lineshapes as a function of temperature.

In the non-cubic phases of these materials (including hexagonal ε-NiIn) the electric field gradient tensor components V_{zz} and η at the atomic sites have been determined from the nuclear quadrupole perturbed ^{27}Al, ^{47}Ti, ^{61}Ni, ^{71}Ga NMR lineshapes together with ^{69}Ga and ^{115}In NQR transition frequencies, and compared with values derived from *ab initio* calculation.

1. Introduction

Notwithstanding the prevalence of nickel as a major constituent in many industrially useful non-ferromagnetic alloys and intermetallics, the use of ^{61}Ni nuclear magnetic resonance (NMR) as an analytical probe in such materials has been limited by its low natural abundance and the low sensitivity of the isotope ($I = 3/2$, 1.1%, 3.8046 MHz T^{-1}). On the other hand the nuclear

quadrupole moment of ^{61}Ni is only moderate, $Q(^{61}\mathrm{Ni}) = 0.162(15) \times 10^{28}$ m^2 $|e|$ [1], and at high fields (∼10 T) this should not be a severe limiting factor. In ionic Ni compounds the magnetic hyperfine broadening caused by the fluctuating electronic moments of the Ni^{2+} ($3d^8$) ions tends to broaden the NMR signal in polycrystalline specimens beyond observability. However, in Ni-based intermetallics for which the Ni 3d shell is filled and Pauli paramagnetism is exhibited, magnetic hyperfine broadening is not an issue and ^{61}Ni NMR spectra are observable, with a reasonable signal to noise ratio being obtained in an hour or less, provided the nuclear quadrupole interaction is not too large.

There have been only a few previous reports of ^{61}Ni NMR in paramagnetic materials: NiAl [2, 3] and NiTi [4, 5]. The work reported below revisits, *inter alia*, both these compounds in greater detail with improved spectral resolution, and substantially extends the range of Ni-based binary intermetallics explored using this spectroscopic method. In addition the nuclear resonance spectroscopy of the counter atom has been investigated and the electric hyperfine interaction, arising from the interaction of the nuclear quadrupole moment with the electric field gradient (efg) at the atom site, has been obtained from the spectra in cases where the Ni or counter atoms are at sites of lower than cubic symmetry.

The intermetallic $Ni_{1-x}Al_x$ has the CsCl structure over the range $0.40 < x < 0.55$. On the Ni-rich side of the equiatomic point ($x = 0.5$) there are Ni substitutions on the Al sublattice; on the Al-rich side there are vacancies on the Ni sublattice which aggregate on Ni (111) planes [6, 7]; in fact at $x = 0.5$ there are constitutional vacancies on the Ni sublattice. As x increases towards $x = 0.6$ a condensation of Ni site vacancies occurs and there is a phase transition involving a distortion of the cubic lattice along [111] to give the trigonal phase Ni_2Al_3 ($P\bar{3}m1$) which, in terms of the parent cubic structure, leaves every third (111) Ni plane vacant. In between NiAl and Ni_2Al_3 an ordered Ni_3Al_4 ($x = 0.571$) vacancy phase has been reported with a cubic cell ($Ia\bar{3}d$) [8]. The orthorhombic $NiAl_3$ phase forms at $x = 0.75$.

$Ni_{1-x}Ga_x$ has the CsCl structure over the range $0.47 < x < 0.52$. At room temperature NiIn is a line compound, hexagonal ($P6/mmm$) [9]. Both Ni_2Ga_3 and Ni_2In_3 are isostructural with Ni_2Al_3. NiTi also has the cubic (CsCl) structure above a critical temperature which is sensitive to very slight changes in the stoichiometry. Below this temperature it undergoes a transformation to a monoclinic structure ($P2_1/m$) [10], referred to as the martensite phase.

Except for NiAl and NiGa, all the intermetallic compounds considered here have atoms at non-cubic positions in the unit cell so that there exists at the atomic site an efg; a tensor quantity specified by V_{zz} and η, where $V_{zz} = \partial^2 V/\partial z^2$ and $\eta = (V_{xx} - V_{yy})/V_{zz}$. Furthermore the atomic nuclei concerned have spin $I \geqslant 3/2$, and therefore a quadrupole moment Q, so that there will be a nuclear quadrupole interaction with coupling constant $C_q(=eV_{zz}Q/h)$ giving structure to the NMR spectrum, enabling C_q to be determined by spectral simulation. Since an accurate (∼1%) value of Q is known for all these nuclei [1], the value of V_{zz} (and η) at the site can be extracted. Using the electronic structure code WIEN 97 [11], theoretical values of V_{zz} and η were computed for the intermetallics investigated below and compared with the experimental numbers (table 2). Recent work [12] has demonstrated that, using the WIEN code, excellent agreement between experimentally and theoretically derived efgs is obtained for a wide range of intermetallics.

The NMR investigation reported here:

(i) Identifies separate components of the ^{61}Ni spectrum for $Ni_{1-x}Al_x$ and attributes them to various defect configurations, which occur for small variations of stoichiometry around NiAl.

(ii) Records the ^{61}Ni Knight shift for $0.4 < x < 0.75$, which includes the ordered compounds NiAl, Ni_2Al_3 and $NiAl_3$.

Table 1. Hyperfine and nuclear quadrupole interaction parameters derived from NMR and NQR lineshapes at 296 K.

Compound	Atom	Nucleus	C_q (MHz)	η	K_{iso} (ppm)	References
NiTi	Ni	^{61}Ni	5.7	0.30	7510	Present work
	Ti	^{47}Ti	∼5.0	∼0.6	3550	Present work
NiIn	Ni	^{61}Ni	6.0	0.67	220	Present work
	In(1)	^{115}In	609.9	0	4200 [a]	Present work
	In(2)	^{115}In	358.2	0	—	
Ni_2Al_3	Al(1)	^{27}Al	16.4	0	545	[3]
	Al(2)	^{27}Al	9.7	0	480	[3]
Ni_2In_3	In(1)	^{115}In	415.5	0	—	—
	In(2)	^{115}In	240.3	0	—	—
Ni_2Ga_3	Ga(1)	^{71}Ga	36.4	0	1530	Present work
		^{69}Ga [b]	57.49	0	—	
	Ga(2)	^{71}Ga	21.6	0	1480	Present work
		^{69}Ga [b]	34.00	0	—	
$NiAl_3$	Al(1)	^{27}Al	8.3	0.85	675	Present work
	Al(2)	^{27}Al	8.9	0.90	978	Present work
Ni_3Al_4	Ni	^{61}Ni	5.0	0.68	140	Present work

[a] From ^{115}In $(1/2, -1/2)$ NMR spectrum.
[b] $Q(^{69}\text{Ga}):Q(^{71}\text{Ga}) = 1.5867$.

(iii) Observes the effect on the ^{61}Ni Knight shift for NiAl and Ni_2Al_3 of replacing Al by the elements Ga and In which have an isoelectronic outer shell with Al.
(iv) Observes the cubic–monoclinic transition in NiTi via the ^{61}Ni and ^{47,49}Ti lineshapes as the temperature is cycled through the transition.
(v) Determines the efg (V_{zz} and η) at the Ni and counter-atom sites from the ^{27}Al, ^{47}Ti, ^{61}Ni, ^{71}Ga NMR lineshapes, and ^{69}Ga and ^{115}In nuclear quadrupole resonance (NQR) transitions of Ni_2Y_3 (Y = Al, Ga, In), $NiAl_3$, ε-NiIn and NiTi (table 1).
(vi) Compares the experimentally derived V_{zz} and η with the values computed using the WIEN code (table 2).

2. Experimental details

The specimens were made by melting the constituent elements together in an argon arc furnace. The resulting ingots were homogenized at temperatures between 600 and 1400 °C for up to 24 h, depending on the melting point, and then crushed and sieved to 160 μm. In some cases the crushed powder was further annealed at an appropriate temperature to remove defects introduced by the crushing. The powder XRD scans of the non-cubic (at ambient lab temperature) materials $NiAl_3$, Ni_2Ga_3, Ni_2In_3 and NiIn indicated that they were highly crystalline and contained approximately 95% of the desired phase. Initial measurements on Ni_2Ga_3 and Ni_2In_3 were made on specimens prepared at Washington State University at Pullman, WA. The compositions referred to in the figures and tables were nominal, as weighed out before melting. Previous experience with Ni aluminides indicated that the Al composition was 0.3–0.5 at.% lower after melting. However, an additional series of Ni–Al alloys, in the range 48–52 at.% Al and in steps of 0.2 at.% Al, had been carefully prepared for a previous ^{27}Al investigation [7]. It was shown that the equiatomic composition was at a nominal 50.7 at.% Al and the present ^{61}Ni work used these samples.

Table 2. Electric field gradients in the non-cubic Ni intermetallics; comparison of computed with NMR-derived values.

Compound	Atom site	$\lvert V_{zz}\rvert_{\text{theor}}$ (V m^{-2})	η	$\lvert V_{zz}\rvert_{\text{expt}}$ (V m^{-2})	η_{expt}
Ni_2Al_3	Ni	0.33	0	< [a]	
	Al(1)	4.32	0	4.61	0
	Al(2)	2.54	0	2.72	0
Ni_2Ga_3	Ni	0.18	0	< [a]	
	Ga(1)	13.34	0	13.9 [b]	0
	Ga(2)	8.03	0	8.22 [b]	0
Ni_2In_3	Ni	0.44	0	< [a]	
	In(1)	22.1	0	21.22	0
	In(2)	14.0	0	12.27	0
$NiAl_3$	Ni	0.42	0.15	< [a]	
	Al(1)	2.06	0.76	2.50	0.90
	Al(2)	2.05	0.59	2.34	0.85
NiIn	Ni	1.91	0.65	1.53	0.67
	In(1) 1a	30.88	0	31.14	0
	In(2) 2d	17.57	0	18.28	0
NiTi	Ni	2.11	0.08	1.40	0.25
	Ti	1.02	0.46	∼0.7	∼0.6

[a] Below detection level.
[b] Derived from ^{69}Ga NQR data.

The ordered defect compound Ni_3Al_4 was prepared by annealing an ingot with the nominal composition $Ni_{42.5}Al_{57.5}$ at 800 °C for 2 h, crushing and sieving to 160 μm powder and annealing the powder for 128 days under argon in a quartz capsule at 560 °C [8]. Subsequent powder XRD indicated well-crystallized material with the presence of some Ni_2Al_3 and NiAl.

The NiTi specimen, provided by NRL, Washington, DC, was prepared by an atomization technique and sieved to 200 μm. Differential scanning calorimetry (DSC) measurements indicated that the cubic–martensitic transition was at about 325 K. Powder x-ray diffraction (XRD) measurements at room temperature indicated that the material was well-crystallized and single phase; essentially all the observed reflections belonged to the low-temperature monoclinic ($P2_1/m$) phase.

Unless separately referenced here, details of all structures are given in *Pearson's Handbook* [13].

The NMR spectrometer was a Bruker Avance 400 operating around 104.2 MHz (^{27}Al), 22.50 MHz (^{47,49}Ti), 35.8 MHz (^{61}Ni), 121.98 MHz (^{71}Ga) and 87.66 MHz (^{115}In) in a nominal field of 9.395 T. The Avance transmitter is broadbanded, simplifying systematic searches for ^{69}Ga and ^{115}In NQR transitions.

Static NMR spectra of the $(1/2, -1/2)$ powder lineshape for ^{27}Al, ^{47,49}Ti, ^{61}Ni, ^{71}Ga and ^{115}In were recorded using a two-pulse echo sequence with pulses spaced between 100 and 350 μs apart, and pulse widths ranging from 1 to 4 μs which excited frequencies with a bandwidth between 1 MHz and 250 kHz about the central frequency. The bandwidth of the loaded probe was about 2 MHz due to eddy current losses in the metal particles. The repetition rate for the pulse sequence was 10 Hz. The whole echo was acquired and Fourier transformed to give the absorption lineshape. The specimen mass was around 500 mg. In general, for ^{61}Ni spectra, 500 000 transients were averaged for a spectrum. However, for stoichiometric, cubic NiAl and NiTi it was sufficient to accumulate of the order of 1000 transients to establish the Knight shift and a good approximation to the linewidth. The ^{27}Al static spectrum for the two non-axial Al sites in $NiAl_3$ proved difficult to interpret and magic angle spinning (MAS) at

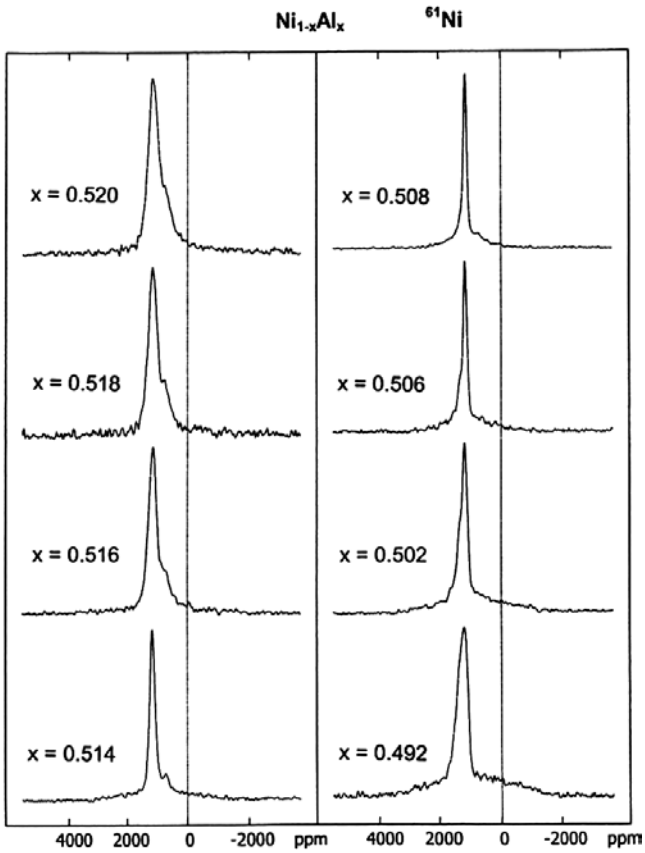

Figure 1. $Ni_{1-x}Al_x$ ^{61}Ni lineshapes for $0.492 \leqslant x \leqslant 0.520$ showing the $x > 0.5$ line and $x < 0.5$ shoulder growing with departure from exact stoichiometry, determined [7] to be at a nominal $x = 0.507$ (see experimental details).

12 kHz, recording single-pulse Bloch decays, was used to remove the Knight shift anisotropy and clearly resolve the two sites.

The NMR and NQR spectra are shown in figures 1–13. The Knight shifts (K_{iso}) for $Ni_{1-x}Al_x$ are plotted in figure 2 and K_{iso} and the derived nuclear quadrupole interaction parameters (C_q and η) for the compounds with non-cubic sites are listed in table 1. The ^{27}Al C_q values for the two axially symmetric Al sites in Ni_2Al_3 have been previously reported [3].

The singular edges of the ^{71}Ga $(1/2, -1/2)$ lineshape for the two Ga sites in Ni_2Ga_3, and the singular edges of the ^{115}In $(1/2, -1/2)$ lineshape for the low-coupling-constant In site in ε-NiIn were recorded by changing the observation frequency to get the edges near the centre of the rf power spectrum. From these partial spectra (not shown here) the ^{71}Ga coupling constants for the two Ga sites and the ^{115}In coupling constant for the low-C_q site in ε-NiIn were obtained.

The analogous singular edges of the ^{115}In $(1/2, -1/2)$ lineshape for the low-coupling-constant site in Ni_2In_3 were not clearly defined.

Guided by the NMR results and WIEN 97 calculations, the probe was removed from the magnet to an approximately field-free area, and the ^{69}Ga $(\pm 1/2, \pm 3/2)$ and three of the four ^{115}In $(\pm m - 1, \pm m)$ NQR transitions for the In sites in both ε-NiIn and Ni_2In_3 were rapidly

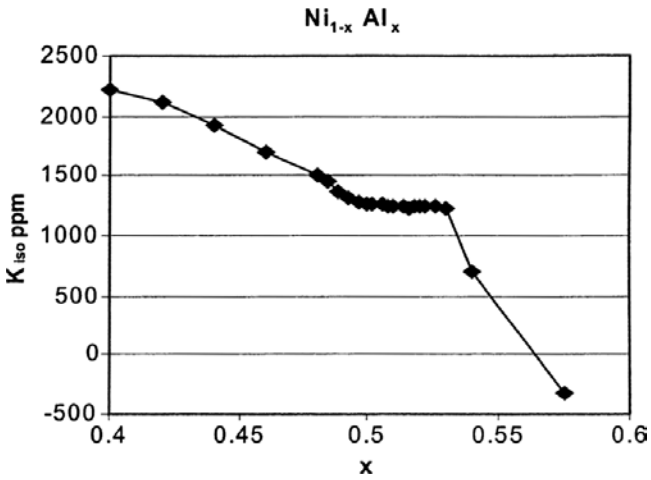

Figure 2. $Ni_{1-x}Al_x$ $K_{iso}(x)$ ^{61}Ni plot for $0.40 \leqslant x \leqslant 0.575$.

located. This yielded substantially more accurate V_{zz} values for the atomic sites concerned. For the two Ga sites in Ni_2Ga_3 and the low-C_q site in ε-NiIn a value of the axial component of the Knight shift tensor (K_{ax}) was obtained from the frequency difference between the estimate of C_q from the simulation of the ^{115}In $(1/2, -1/2)$ lineshape (assuming only nuclear quadrupole interaction) and the essentially exact value derived from the NQR transition frequencies. For the low-coupling-constant counter-atom site in Ni_2Ga_3 and Ni_2In_3 the NQR lines were very broad, of order the excitation width of the rf pulse, and care was taken to check that the peak position of the recorded line moved correctly when the offset frequency was changed.

It should be noted explicitly at this stage that for Ni_2Ga_3 and Ni_2In_3 (and for ε-NiIn) the accuracy of the V_{zz} predictions from WIEN 97 can be turned to good use by drastically limiting the frequency scanning range necessary to locate the ^{69}Ga and ^{115}In NQR transitions. For Ni_2Ga_3 the WIEN 97 predictions of the ^{69}Ga NQR transitions (via V_{zz}(Ga)) matched the accuracy by which they could be derived from the NMR determination of C_q(^{71}Ga).

Lineshape simulations of the NMR spectra to give C_q, η were performed using the program DMFIT [14].

The temperature of the specimen in the probe for the NMR spectra was 296 K; for the NQR spectra with the probe out of the magnet the specimen temperature was 294 K.

NMR reference shift zeros were obtained from aqueous $Al(NO_3)_3$ (^{27}Al), the cubic perovskite $SrTiO_3$ (^{47,49}Ti), GaAs (^{71}Ga) and InP (^{115}In). For ^{61}Ni a synthetic zero shift was derived from a resonance frequency for ^{35}Cl (using NaCl(aq)) and the known ratio of the ^{61}Ni and ^{35}Cl nuclear magnetic moments.

3. Results and discussion—Ni site

3.1. $Ni_{1-x}Al_x$

The cubic CsCl structure is maintained from $x = 0.40$ to about $x = 0.56$. Very close to the equiatomic NiAl on the Al-rich side, there appeared an additional small line with lower K_{iso} which soon merged, with increasing Al content, into the wings of the line from the B2 phase (figure 1). Since on the Al-rich side of equiatomic there are vacancies on the Ni sublattice [6] this line is attributed to next-nearest-neighbour Ni sites which octahedrally coordinate the Ni vacancy.

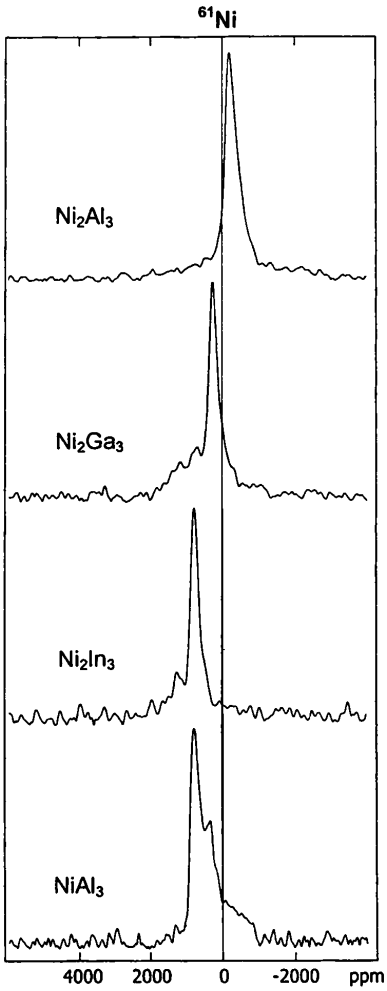

Figure 3. Ni_2Al_3, Ni_2Ga_3, Ni_2In_3 and $NiAl_3$ ^{61}Ni lineshapes.

At $x = 0.575$ the specimen which had been rapidly quenched after melting exhibited a sharp Ni_2Al_3 line and a broad background indicating a disordered phase: annealing at 850 °C removed the Ni_2Al_3 line and resulted in a broad, roughly triangular, lineshape peaked at lower K_{iso} than that for Ni_2Al_3. This line is possibly the disordered vacancy precursor stage of the compound Ni_3Al_4 [8]. The ^{61}Ni spectrum from ordered Ni_3Al_4 is discussed below.

On the Ni-rich side of equiatomic a shoulder appears on the high-frequency side of the main ^{61}Ni line and is attributed to Ni antisites (i.e. Ni $\rightarrow$ Al) and the eight nearest-neighbour Ni sites which directly coordinate the antisite. On further increasing the Ni content this shoulder merges into the broadening main line. Similar antisites have been observed in a series of slightly aluminium rich γ-TiAl [15] as a resolved line in the ^{27}Al spectrum with an intensity which increased as the Al excess increased.

At $x = 0.40$ a specimen which was rapidly quenched after melting exhibited a minor component line from the cubic phase and a broad non-Gaussian background component. Annealing at 1000 °C left this composite lineshape unchanged. The background did not

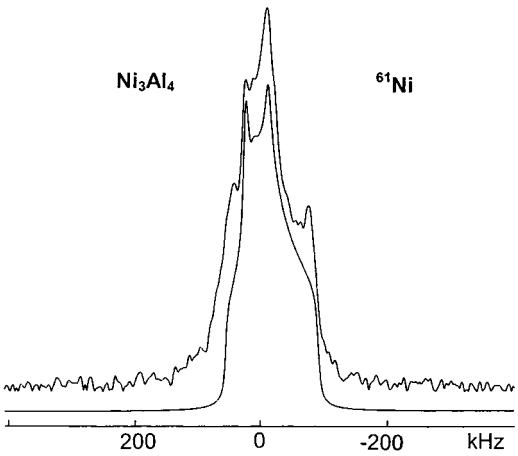

Figure 4. Ni_3Al_4 ^{61}Ni lineshape and simulation (smooth curve, below).

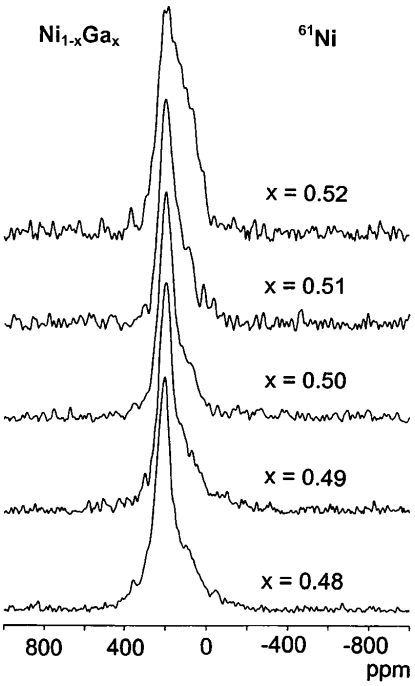

Figure 5. $Ni_{1-x}Ga_x$ ^{61}Ni lineshapes for $x = 0.48$–0.52.

exhibit any suggestion of structure that might indicate the presence of an ordered phase with composition Ni_3Al_2 [13].

3.2. Knight shift change in $Ni_{1-x}Al_x$ with varying stoichiometry: $K_{iso}(x)$

On increasing x from 0.40, and remaining in the B2 (cubic) phase region, the ^{61}Ni Knight shift for the identified cubic phase component decreases rapidly but is stationary from approximately $x = 0.50$ to 0.53 and subsequently drops rapidly (figure 2). The line broadens rapidly

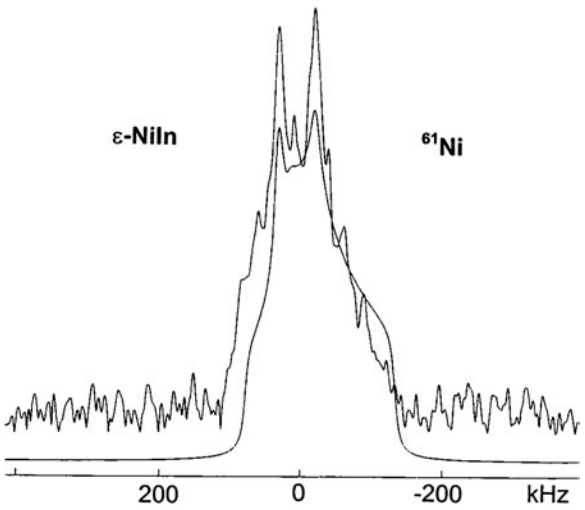

Figure 6. ε-NiIn ^{61}Ni lineshape and simulation (smooth curve, below).

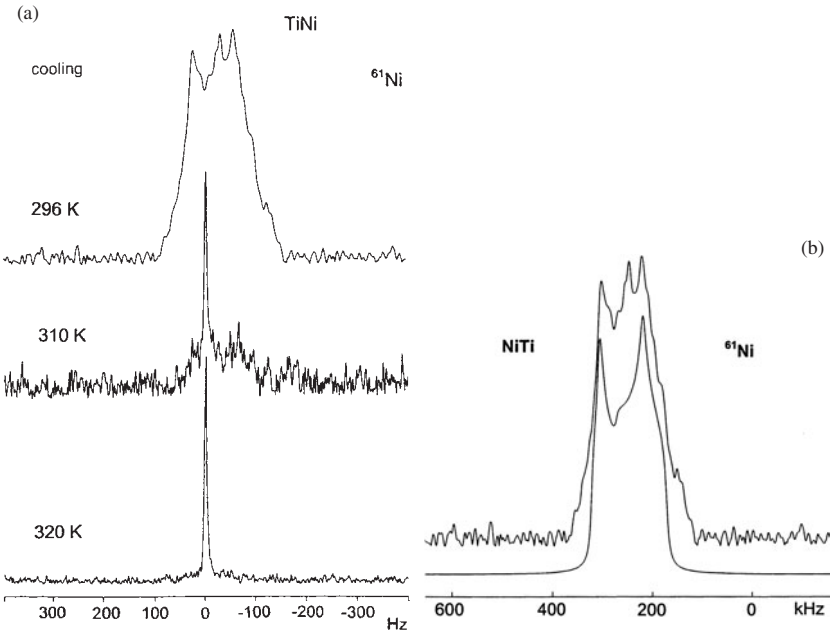

Figure 7. NiTi ^{61}Ni lineshape (a) in the cubic phase at 320 K, at 310 K and 296 K—data taken on cooling the specimen; (b) in the martensitic phase (at 296 K) lineshape and simulation (smooth curve, below).

for compositions away from equiatomic. Near equiatomic the B2 line can be resolved separately from the antisite lines and K_{iso} clearly identified. For larger x excursions the defect contributions are not clearly separable from the B2 line, and K_{iso} is taken as the shift for the line peak. For $x = 0.575$ the 'as-quenched' specimen exhibited a lineshape indicating that the specimen contained a major Ni_2Al_3 component (i.e. $x = 0.60$). On annealing at

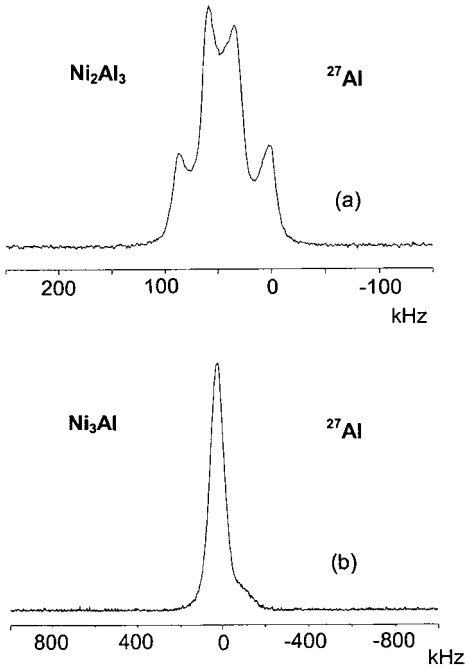

Figure 8. ^{27}Al NMR lineshape for (a) Ni_2Al_3 indicating contributions from Al(1) and Al(2); (b) Ni_3Al.

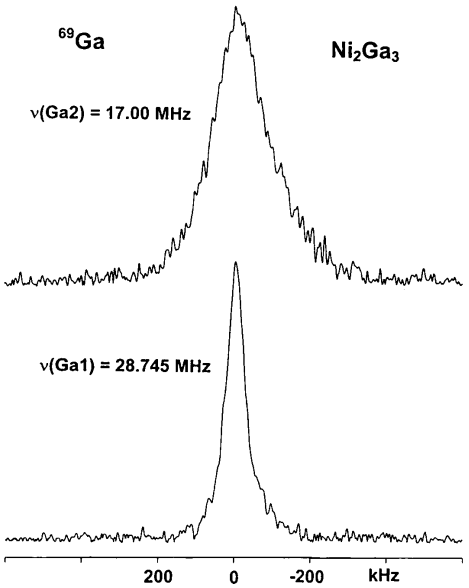

Figure 9. Ni_2Ga_3 ^{69}Ga NQR ($\pm 1/2$, $\pm 3/2$) transition lineshapes for (bottom) Ga(1) and (top) Ga(2).

850 °C for 20 h the Ni_2Al_3 component disappears and the lineshape becomes much broader and asymmetric, peaking at a shift clearly lower than that for Ni_2Al_3. An orthorhombic ordered defect phase Ni_3Al_4 ($x = 0.571$) has been reported [8], requiring long annealing to achieve

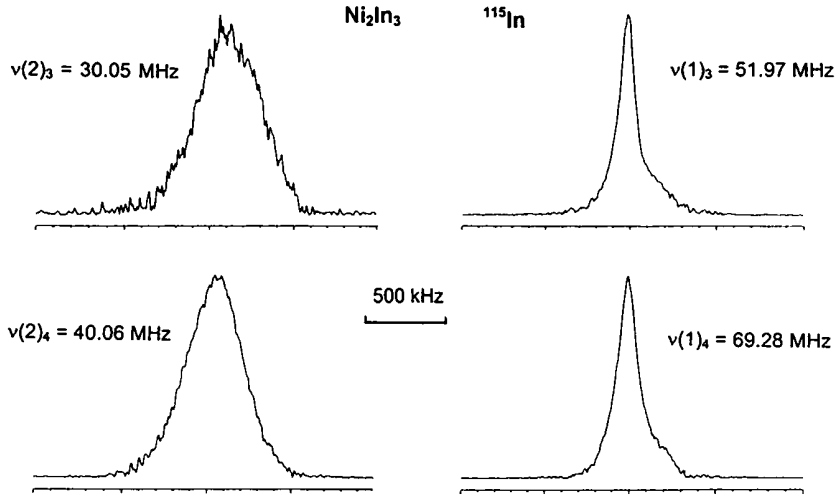

Figure 10. Ni_2In_3 ^{115}In NQR ($\pm 5/2$, $\pm 7/2$) and ($\pm 7/2$, $\pm 9/2$) transition lineshapes for (right) In(1) and (left) In(2).

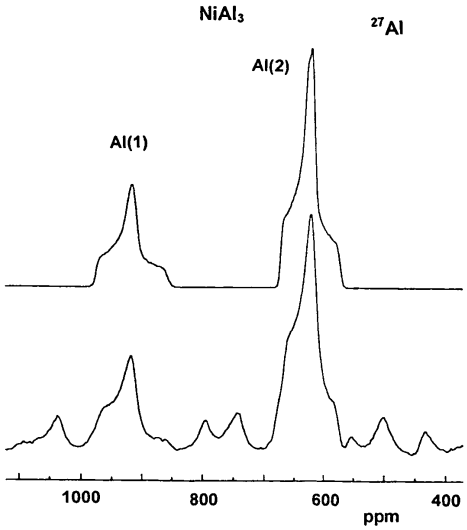

Figure 11. $NiAl_3$ ^{27}Al MAS lineshapes (bottom) and simulation (top).

complete atomic ordering. This lineshape presumably indicates the initial stages of formation of this phase.

Recall that for Ni-rich NiAl there are Ni substitutions on the Al sublattice and that for Al-rich NiAl there are vacancies on the Ni sublattice. If it is assumed, as a crude approximation, that the volume occupied by a Ni atom, an Al atom and a vacancy are the same, and that each Al atom added after $x = 0.5$ generates a vacancy, then it can be seen that the valence electron to atom ratio (e/a) peaks at $x = 0.5$ and decreases linearly from this maximum on either side of $x = 0.5$. The change in sign of the slope of e/a at $x = 0.5$ is apparently sufficient to temporarily arrest the decrease in K_{iso} as x approaches 0.5 from below before the approach of another phase, Ni_2Al_3 or Ni_3Al_4.

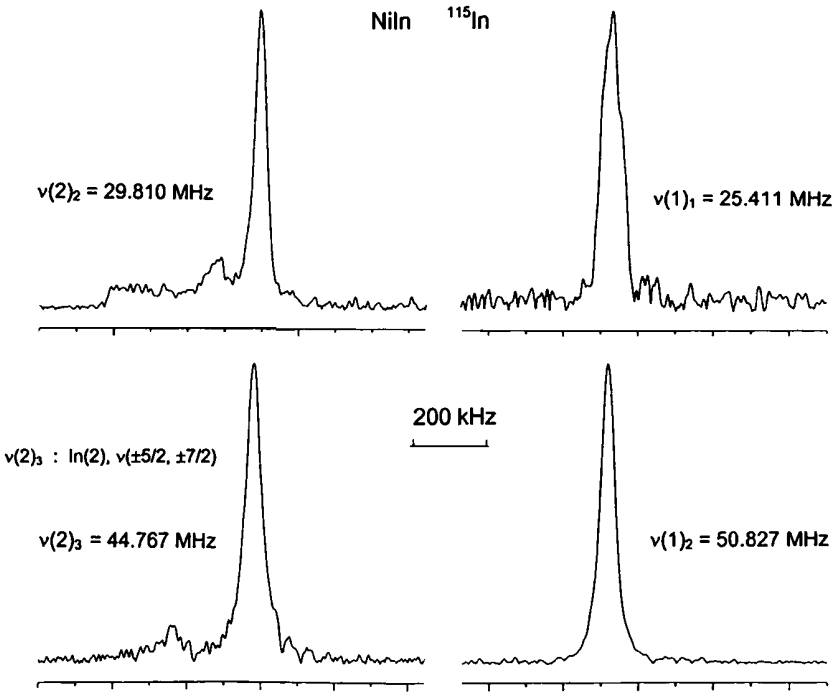

Figure 12. NiIn ^{115}In NQR lineshapes for ($\pm 3/2$, $\pm 5/2$) and ($\pm 5/2$, $\pm 7/2$) transitions for (left) In(1) and (right) In(2).

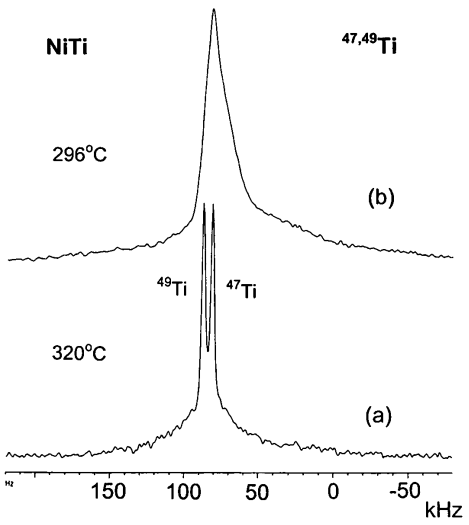

Figure 13. NiTi ^{47,49}Ti lineshape in (a) the cubic phase at 320 K and (b) in the martensitic (monoclinic) phase at 296 K.

In the $Ni_{1-x}Al_x$ series, no structure analogous to that reported above for ^{61}Ni is observed in the ^{27}Al lineshape [3], where the ^{27}Al line merely broadens for small deviations from $x = 0.5$. Ni appears a more sensitive observer of substitutional and vacancy defects in $Ni_{1-x}Al_x$ than Al.

Certainly Ni is a nearest-neighbour observer of substitutions on the Ni sites, but Al is the nearest neighbour of a vacancy on the Ni sites. The enhanced resolution is possibly due to larger contact interaction at the Ni nucleus giving rise to a more amplified change in Knight shift per given change in s-electron density at the nucleus $|\psi(0)|^2$. It may also be due to the low value of V_{zz}(Ni) at the B2 phase Ni and the Ni at or near the defect which leads to relatively sharp, and therefore resolved, ^{61}Ni lines.

3.3. Ni_2Al_3, Ni_2Ga_3 and Ni_2In_3

These isostructural compounds are trigonal ($P\bar{3}m1$) and can be described as being derived from the cubic NiY (CsCl type) structure by removing every third Ni (111) plane and adding an axial distortion along ⟨111⟩. This yields one Ni site and two distinguishable Y sites (Y = Al, Ga, In) in the unit cell: Y1 in 1a and Y2 in 2d. Both sites have 3-fold axial symmetry so that the efg tensor is described simply by the largest component in the principal axis frame V_{zz}, with the asymmetry parameter $\eta = (V_{xx} - V_{yy})/V_{zz} = 0$. The ^{61}Ni spectra are displayed in figures 3(a)–(c). Note the increase in $K_{\rm iso}$ with increasing mass of the group III substituent. Note also the narrow ^{61}Ni lines recorded for non-cubic Ni sites in the Ni_2Y_3 compounds despite the existence in principle of an efg. WIEN 97 calculations gave values for V_{zz}(Ni) which set a lower limit to linewidth. The reliability of these values can be gauged by the excellent agreement obtained between NMR experiment and WIEN 97 theory for V_{zz} at the counter-atom sites (table 2).

3.4. $NiAl_3$

For orthorhombic $NiAl_3$ ($Pnma$) with one distinguishable Ni atom in the unit cell, extra structure was observed in the ^{61}Ni spectrum (figure 3). WIEN 97 computations of V_{zz}(Ni) indicate a low value (table 2) and thus a single narrow line was expected. Despite homogenization of the ingot (at 750 °C), and further annealing of the powder at the same temperature, XRD trace indicates the presence of Ni_2Al_3 which accounts for the step (or shoulder) in the lineshape at the most negative shift value. A preliminary ^{61}Ni specimen crushed from an as-cast ingot of $NiAl_3$ stoichiometry yielded an additional very strong line at the Ni_2Al_3 shift. This Ni_2Al_3 component was considerably attenuated by homogenization of the ingot and annealing the crushed powder. The shoulder structure on the low-shift side of the main $NiAl_3$ line may be due to Ni → Al antisites or other well-defined defect sites around Ni sites. An attempt to simulate the shoulder structure by adding a Knight shift anisotropy component to the simulation parameters was unsuccessful.

3.5. Ni_3Al_4

The ordered compound Ni_3Al_4 exhibited the second-order quadrupole perturbed ^{61}Ni spectrum shown in figure 4. The feature at approximately 1150 ppm (or 41.2 kHz) appears to be slightly Al-rich NiAl in accord with the XRD scan. Similarly, part of the width of the low-frequency peak of the main spectrum near −370 ppm is due to Ni_2Al_3. A reasonable fit to the spectrum indicated $C_{\rm q} = 5.0$ MHz and $\eta = 0.68$.

3.6. Ni_3Al

No compact ^{61}Ni lineshape was observed in Ni_3Al, despite homogenizing the ingot for 1 week at 1000 °C and annealing the powder specimen at 1200 °C for 2 h. A very weak ^{61}Ni echo was observed at several arbitrary frequencies around the $K_{\rm iso}$ value for NiAl, with frequency

width $\approx$(pulse width)$^{-1}$, indicating the presence of a very broad line, very much broader than that predicted by WIEN 97, which is usually a reliable guide. A very dispersed line may be attributed to the presence of ferromagnetically ordered $(Ni)_n$ clusters [16] which would cause magnetic hyperfine broadening.

3.7. $Ni_{1-x}Ga_x$

Five x values were investigated—nominal equiatomic and two x values on either side: $x = 0.48$, 0.49, 0.50, 0.51 and 0.52. The ^{61}Ni Knight shift at the equiatomic composition was 2055 ppm compared with 1250 ppm for equiatomic NiAl. The ^{61}Ni line was narrowest for $x = 0.50$ and broadened asymmetrically on the low-frequency side for both $x > 0.5$ and $x < 0.5$, presumably because of the presence of a line due to defect formation (figure 5). Compare the case of $Ni_{1-x}Al_x$ where the ^{61}Ni shifts for the Al vacancy ($x > 0.5$) and Ni substitution ($x < 0.5$) lines are on opposite sides of the main line. If the same interpretation is used for $Ni_{1-x}Ga_x$ the defect line is due to Ga vacancies.

3.8. NiIn

The cubic phase of NiIn is only stable above $\sim$850 °C. At room temperature the stable phase, ε-NiIn, is trigonal ($P6/mmm$) with one Ni site (in 3f) and two distinguishable In sites (in 1a and 2d) [9]. Note that the point symmetry of the Ni atom is mmm so that there will be a non-zero asymmetry parameter for the efg. A powder specimen of nominally equiatomic NiIn, annealed at 600 °C for 2 h, and shown by powder XRD to consist of >95% trigonal ε-NiIn with excellent crystallinity, yielded the ^{61}Ni spectrum shown in figure 6. Lines at 830 and -585 ppm are prominent, accompanied by broad wings. Assuming that this structure is that of a second-order quadrupolar lineshape, a simulation yielded $C_q = 6.0$ MHz ($V_{zz} = 1.53 \times 10^{21}$ V m^{-2}), and $\eta = 0.67$. WIEN 97 computations yielded $|V_{zz}(\mathrm{Ni})| = 1.91 \times 10^{21}$ V m^{-2} and $\eta = 0.65$.

3.9. NiTi

The sharp ^{61}Ni line (FWHM = 5 kHz) observed in the cubic phase (figure 7(a)) indicated that the material was essentially strain free. In the low-temperature monoclinic (martensite) phase the line was broad, with clear second-order quadrupolar structure (figure 7(b)). An extra peak at 6800 ppm (243 kHz) was visible near the centre of the lineshape. From the shift it is clear that this extra peak is not due to residual cubic B2 phase; it may possibly be due to a small volume of a pre-martensitic phase. The completeness with which the XRD spectrum could be fitted by the monoclinic martensite phase d-spacings argues against a major impurity phase. The trigonal (space group P3) NiTi R-phase [17], which mediates the transition between the high-temperature cubic phase and the low-temperature monoclinic phase, was considered as a possible candidate, but rejected as unlikely on the basis of WIEN 97 computation of an appreciable efg at the three Ni sites.

A simulation of the main ^{61}Ni lineshape yielded a value for the nuclear quadrupole coupling constant $C_q = eQV_{zz}/h$ and asymmetry parameter η. The efg V_{zz} was independently calculated using the XRD structure [10]. The experimental value of V_{zz} and η was evaluated using the published value of $Q(^{61}\mathrm{Ni})$ [1]; the theoretical values are in reasonable agreement (table 2).

The transition between the two phases was monitored by both the ^{61}Ni and ^{47,49}Ti spectra. Despite some thermal inhomogeneity over the specimen in the variable-temperature probe the transition was sharp; an approximate 10 °C hysteresis was observed on thermal cycling between the high- and low-temperature phases.

The difference in the ^{61}Ni lineshape in NiTi at temperatures well above and well below the transition has previously been observed using a frequency-stepped echo method [4]. However, the resolution was lower, especially in the cubic phase (possibly due to residual strains in the sample), and some interpretation was necessarily different in that the lineshape observed below the cubic phase transition was essentially Gaussian with an admixture of residual cubic phase line.

4. Results and discussion—counter-atom site

4.1. Ni_2Al_3, Ni_2Ga_3 and Ni_2In_3

The crystal structure of the Ni_2Y_3 compounds requires two distinguishable Y sites, i.e. a separate efg at each Y site. This multiplicity is clearly exhibited by nuclear resonance and two axially symmetric efg components are observed in the ^{27}Al and ^{71}Ga NMR and ^{115}In NQR spectra with the two C_q in an approximate ratio of 1:1.7.

A clear basis for the allocation of each coupling constant to its specific site is seen in the case of Ni_2Al_3 (figure 8(a)) where the outer two peaks belong to the second-order quadrupole perturbed lineshape corresponding to Al(1) and the inner two peaks belong to that for Al(2). The integrated intensity ratio of the two contributing lineshapes is approximately 1:2. This indicates that the large C_q site is Al(1) and the small C_q site is Al(2). From the C_q values and the quadrupole moment for ^{27}Al, the V_{zz} at the two sites (table 1) can be obtained and compared with the theoretically computed value (table 2); it can be seen that experimental and theoretical values are in excellent agreement.

Because of its large frequency width ($\sim$1.4 MHz), due to increased nuclear quadrupole coupling, the ^{71}Ga spectrum for Ni_2Ga_3 was obtained in sections. Four separate scans at different offset frequencies (not displayed here) recorded the location of the pair of singular edges of the $(1/2, -1/2)$ lineshape for the two Ga sites. The two C_q values derived from the edge frequencies are given in table 1. From $C_q(^{71}\text{Ga})$ the values of $C_q(^{69}\text{Ga})$ were derived from the known ratio $^{69}Q{:}^{71}Q = 1.5867$. The ^{69}Ga NQR transition frequencies for Ga(1) and Ga(2) were then derived: $\nu(\pm 1/2, \pm 3/2) = \nu_q = C_q/2$. These transitions were then observed by measurements in zero external magnetic field at frequencies very close to those predicted from NMR. The transition lineshapes for each site are displayed in figure 9. It can be seen that the linewidth (FWHM) for the Ga(2) site is more than three times the width of the Ga(1) site. It is noticeable that the lineshapes are distinctly Lorentzian in character which may indicate the onset of intersite Ga(1) $\leftrightarrow$ Ga(2) hopping at room temperature of the kind observed, in the fast hopping limit, in Ni_2Al_3 at elevated temperatures [3]. Abragam [18] gives a derivation for the analogous solid phase NMR lineshape which is Lorentzian in the fast hopping limit.

For Ni_2In_3 the coupling was sufficiently large that measurements in zero field (i.e. NQR) for the ^{115}In $(\pm m - 1, \pm m)$ NQR transitions were necessary to determine the C_q for the two In sites. The search was commenced from a starting frequency derived from the WIEN 97 prediction and the observed transitions were then rapidly located. The quality of the prediction can be appreciated from inspection of tables 1 and 2. The $(\pm 5/2, \pm 7/2)$ and $(\pm 7/2, \pm 9/2)$ transitions for the two In sites, at frequencies $3C_q/14$ and $4C_q/14$ respectively, are displayed in figures 10 (right) and (left). It is noticeable that the resonances for the low-C_q site (figure 10 (left)) are at least four times the width of the resonances for the high-C_q site (figure 10 (right)). As for Ni_2Ga_3 the ^{115}In lineshapes have a marked Lorentzian character and a similar hopping argument (see previous paragraph) may apply.

For Ni_2Ga_3 and Ni_2In_3, by analogy with Ni_2Al_3, the site with the smaller coupling constant was allocated to Ga(2) and In(2) respectively and the higher C_q site to Ga(1) and In(1), an allocation which is nicely confirmed by the computed V_{zz} values (table 2).

The considerably wider distribution of V_{zz} around the peak value for Ga(2), In(2), compared to that for Ga(1), In(1), which is indicated in the NQR linewidths, is consistent with the (2) site being adjacent to the 'vacant' layer. In an imperfect preparation this layer may in fact contain interstitial atoms and be the source of some crystallographic disorder felt directly by the (2) site, but only indirectly by the Ga(1) site.

Similar allocation of coupling constants to sites for Ni_2Ga_3 and Ni_2In_3 maintains this excellent agreement between experiment and theory, as can be seen from table 2.

4.2. $NiAl_3$

This compound is orthorhombic with two distinguishable Al sites in the unit cell of multiplicity 1 and 2 respectively. As noted above, the static ^{27}Al spectrum proved difficult to interpret and a magic angle spinning (MAS) spectrum (figure 11) proved necessary to extract the C_q, η values for the two sites. Two MAS lineshapes were resolved indicating sites with high values of η. The relative intensities make it clear that the lineshape with the smaller $^{27}K_{iso}$ and smaller C_q belongs to the site with multiplicity 2. In this case the computed V_{zz} and η for the two sites are correctly close in each case, but lower than the measured values, in the case of the V_{zz} by 18% and 12% respectively. It is not known how reliable the reported crystal structure is [16].

4.3. Ni_3Al_4

The static ^{27}Al spectrum revealed a relatively narrow (about 45 kHz FWHM) unstructured central component and some very broad and featureless satellites. MAS at 12.5 kHz failed to provide a clearer spectrum.

4.4. Ni_3Al

A ^{27}Al NMR investigation of this material has previously been reported by Scherrer *et al* [16]. In the present work a similar spectrum to that shown in [16] is observed (figure 8(b)). The small shoulder on the low-frequency side of the main line may be due to a defect site. Similar structure has been observed in ^{27}Al spectra for a series of cubic (B2) $Fe_{1-x}Al_x$ intermetallics as x was varied from $x = 0.5$ to 0.46 [19].

4.5. ε-NiIn

Unlike NiAl and NiGa which have the cubic CsCl structure at room temperature, NiIn is trigonal at room temperature [9], and only attains the cubic form above 800 °C. The two distinguishable In atoms are in sites of multiplicity 1 and 2 respectively with at least 3-fold axial symmetry, ensuring $\eta = 0$. The edge singularities for the ^{115}In NMR $(1/2, -1/2)$ lineshape of one of the sites were located approximately 9.5 MHz apart. Calculating C_q and thus V_{zz} from this separation, and guided by the WIEN 97 computation, this C_q was allocated to the site with In in 2d. A brief search in zero field, guided by the theoretical prediction, located three of the four NQR transitions for In in 1a and for In in 2d. The lineshapes for two of the transitions for each site are shown in figure 12. The measured transition frequencies overdetermine the coupling constant in each case and independently establish $\eta = 0$ for both sites from the strict harmonic ratio of the frequencies. The V_{zz} values computed by WIEN 97 are in excellent agreement with the experimentally determined values (see table 1).

It is worth emphasizing that the accurate theoretical predictions of the experimentally determined C_q (or V_{zz}) achieved here depend on the quality of the electronic structure code

and the accuracy of the structural parameters (especially the atomic positions) and the nuclear quadrupole moments.

Note that the approximate value of ν_q (=14.1 MHz) obtained from the NMR spectrum was derived purely from the frequency separation from the two singular edges; a method which ignored the contribution to the $(1/2, -1/2)$ lineshape from the axial component of the Knight shift tensor (K_{ax}). The latter quantity also contributes to the lineshape and accounts for the difference between the estimate and the exact value derived from NQR. This difference can be used to derive the Knight shift anisotropy, either from DMFIT or by using the expression [20]

$$K_{ax} = 5\nu_q(\pm\nu'_q - \nu_q)/\nu_L^2$$

where ν'_q is the estimate from the lineshape simulation ignoring K_{ax}, ν_q is the exact value derived from NQR and ν_L is the Larmor frequency. This gives $K_{ax} = 7950$ ppm.

4.6. NiTi

The abundance and NMR sensitivity of the isotopes ^{47,49}Ti, while larger than for ^{61}Ni, is still considerably less than that for ^{27}Al, ^{69,71}Ga and ^{115}In. However, ^{47,49}Ti has been shown to be a structurally revealing probe for Ti-based intermetallics [21, 22].

For NiTi the difference between the cubic and monoclinic phase was almost as sharply defined in the ^{47,49}Ti spectrum as in the ^{61}Ni spectrum. In the cubic phase at 320 K two peaks are visible—the high-frequency peak is due to ^{49}Ti and the low-frequency peak to ^{47}Ti (figure 13(a)). The magnetic moments of the two isotopes are such that the separation between the peaks is 6 kHz at a field of 9.4 T. In the monoclinic phase at (296 K) a quadrupolar interaction broadens the line for each isotope and a superposition of the lineshape for ^{49}Ti within that for ^{47}Ti is the result (figure 13(b)).

A rough value of V_{zz} and η at the Ti site in the monoclinic phase was derived from figure 13(b) by simulation of the lineshape, and the values are listed in table 2.

5. Conclusions

It has been demonstrated that ^{61}Ni in natural abundance can be used as a practical probe for paramagnetic Ni-based intermetallics using pulsed Fourier transform NMR at room temperature. Further, the ^{61}Ni Knight shift has been shown to be usefully sensitive to stoichiometry and defect structure in Ni–Al, Ni–Ga binary intermetallics: in particular the observation of two clearly defined lattice defect lines appearing on either side of the main ^{61}Ni line for very small deviations from the equiatomic NiAl composition.

The efg data from ^{61}Ni and the counter-atom nucleus NMR probes provide a compact index of the correctness of the crystal structure of these intermetallics, since it has been established that the WIEN 97 code yields accurate electronic structures (and thus V_{zz}, η) provided the crystal structure is precisely determined. These computed efg parameters in turn enable rapid location of high-precision zero-field (NQR) transitions.

Acknowledgments

We are grateful to Pavla Meakin for the DSC analysis of the NiTi specimen, to Liz Goodall for the powder XRD analysis, and to Gary Collins and Matthew Zacate for the Ni_2Ga_3 and Ni_2In_3 specimens on which the preliminary measurements were made. We also thank Irek Kozicki for providing a salt bath at 560 °C for the 4 month annealing of Ni_3Al_4.

References

[1] Pyykkö P 2001 *Mol. Phys.* **99** 1617
[2] Drain L E and West G W 1965 *Phil. Mag.* **11** 1061
[3] Bastow T J, Smith M E and West G W 1997 *J. Phys.: Condens. Matter* **9** 6085
[4] Crevoiserat S, Scherrer P, Dimitropoulos C and Gotthardt R 1999 *Mater. Sci. Eng.* A **273–275** 357
[5] Crevoiserat S, Dimitropoulos C and Gotthardt R 2002 *Mater. Trans.* **43** 785
[6] Bradley A J and Taylor A 1937 *Proc. R. Soc.* A **159** 56
[7] West G W 1973 *Phys. Status Solidi* a **20** 647
[8] Ellner M, Kek S and Predel B 1989 *J. Less Common Met.* **154** 207 [Ni3Al4]
[9] Fischer R A, Kleine M, Lehman O and Stuke M 1995 *Chem. Mater.* **7** 1863
[10] Bührer W, Gotthardt R, Kulik A, Mercier A and Staub F 1983 *J. Phys. F: Met. Phys.* **13** L77
[11] Blaha P, Schwarz K and Luitz J 1999 *WIEN 97, A Full Potential Linearized Augmented Plane Wave Package for Calculating Crystal Properties* Technical University of Vienna ISBN 3-9501031-0-4
This is an improved and updated Unix version of the original copyrighted WIEN code, which was published by Blaha P, Schwarz K, Sorantin P and Trickey S B 1990 *Comput. Phys. Commun.* **59** 399
[12] Bastow T J, Burgar M I and Maunders C 2002 *Solid State Commun.* **122** 629
[13] Villars P and Calvert L D (ed) 1985 *Pearson's Handbook of Crystallographic Data for Intermetallic Phases* (Metals Park, OH: American Society for Metals)
[14] Massiot D, Fayon F, Capron M, King I, Le Calvé S, Alonso B, Durand J-O, Bujoli B, Gan Z and Hoatson G 2002 *Magn. Reson. Chem.* **40** 70–6
[15] Smith M E, Gibson M A, Forwood C T and Bastow T J 1995 *Phil. Mag.* A **74** 791
[16] Scherrer P, Dimitropoulos C, Borsa F and Rubini S 1998 *Phys. Rev.* B **57** 10462
[17] Hara T, Ohba T, Okunishi E and Otsuka K 1997 *Mater. Trans. JIM* **38** 11
[18] Abragam A 1961 *The Principles of Nuclear Magnetism* (Oxford: Oxford University Press) p 439
[19] Bastow T J 2003 MS in preparation
[20] Baugher J F, Taylor P C, Oja T and Bray P J 1969 *J. Chem. Phys.* **50** 4914
[21] Bastow T J, Forwood C T and Gibson M A 1998 *Solid State Nucl. Magn. Reson.* **12** 201
[22] Bastow T J, Forwood C T, Gibson M A and Smith M E 1998 *Phys. Rev.* B **58** 2988